Teng, Y. *et al*. (2020). *Géotechnique* **70**, No. 12, 1083–1093 [https://doi.org/10.1680/jgeot.18.P.058]

Mechanisms beneath rectangular shallow foundations on sands: vertical loading

YINING TENG*†, SAM A. STANIER‡ and SUSAN M. GOURVENEC§

This paper details analysis of deformation behaviour of silica and carbonate sands under a rectangular foundation subject to uniaxial vertical load based on results from a series of centrifuge model tests. A multiscale particle image velocimetry/digital image correlation (PIV/DIC) technique was used to record and analyse the foundation tests with high resolution and measurement precision. Cone penetrometer and pressuremeter tests provide in situ soil characterisation of the tested sand sample in the centrifuge environment. The soil behaviour is analysed through foundation load–settlement response and the observed soil deformation measurements. Different soil deformation mechanisms and strain behaviours were observed in the different sands tested, and the particle shape effect is considered, with data from scanning electron microscopy, to explain the differences. The results and analyses contribute towards better understanding of different soil behaviours under shallow foundations in different sands.

KEYWORDS: calcareous soils; centrifuge modelling; footings/foundations; in situ testing; particle crushing/crushability; soil/structure interaction

INTRODUCTION

Soil response in sands of different mineralogy is known to vary significantly. In particular, silica and carbonate sands, which are prevalent offshore in the continental margins, often exhibit contrasting behaviour in element tests, with carbonate sands highly susceptible to large volumetric collapse (e.g. Frossard, 1979; Coop *et al*., 2004; Cho *et al*., 2006). This is because natural carbonate sands are characterised by high variability in soil properties compared to silica sands, due to the biogenic origin of carbonate sands, high angularity of particles and variable particle strength leading to a tendency to crush. Attempts to capture some of these behaviours in constitutive models include the MIT-S1 model (Pestana, 1994) and SU model (Islam, 1999); however, most soil models do not consider particle shape effects or crushability. Such models are not used routinely in the design of foundations on carbonate sands, with traditional bearing capacity theories still very much relied upon that are based on a general shear failure mechanism with the soil being treated as a homogeneous continuum (Terzaghi, 1943; Meyerhof, 1951; Hansen, 1970).

For reliable and economic design, it is important to understand whether particle shape effects and crushability of carbonate sands have an impact on the validity of traditional bearing capacity theory. Research into the effect of this varying mechanical behaviour on the deformation mechanisms that are mobilised in boundary value problems – such as shallow foundation performance – is sparse in the literature (e.g. Dijkstra *et al*., 2013; Teng, 2018). Shallow foundation tests on sand in a centrifuge environment, in which the stresses are scaled appropriately, are reported in the literature (e.g. Bolton *et al*., 1999; Zhu *et al*., 2001; Govoni *et al*., 2011; Cocjin & Kusakabe, 2013; Teng *et al*., 2017), yet most of the studies use well-characterised 'laboratory' sands, which are typically rounded, uniformly graded siliceous sands that are commercially available in the reasonably large volumes required for centrifuge model studies.

This paper details a series of shallow foundation tests on a commercially available siliceous sand and two natural carbonate sands in the centrifuge environment, using a multi-scale particle image velocimetry/digital image correlation (PIV/DIC) technique to record the evolving deformation mechanisms caused by the foundation load at both the micro and macro scale. Complementary cone penetrometer tests and pressuremeter tests were also carried out. The observations indicate that the particle shape effect and crushability have a significant impact on shallow foundation response in sand of differing origin; this is a factor which should be carefully considered when designing shallow foundations that are to be founded on atypical and poorly characterised sediments.

EXPERIMENTAL DETAILS

Two types of centrifuge tests (illustrated in Fig. 1) were performed: (*a*) half-model PIV/DIC experiments in a reduced-sized PIV strongbox with a transparent acrylic window set into a standard full-size strongbox; and (*b*) full-model tests performed in a full-size strongbox to verify the load measurements obtained in the PIV/DIC experiments and provide additional space for in situ sample characterisation tests. All experiments were performed in the 1·8 m radius beam centrifuge at the University of Western Australia (UWA) (Randolph *et al*., 1991) with an acceleration of 50***g*** applied at the surface of the sample. The measurements were recorded with the LabView based DigiDAQ software developed at UWA (Gaudin *et al*., 2009).

Manuscript received 11 March 2018; revised manuscript accepted 27 August 2019. Published online ahead of print 27 September 2019. Discussion on this paper closes on 1 April 2021, for further details see p. ii.

* Norwegian Geotechnical Institute, Oslo, Norway (Orcid:0000-0002-0907-1409).
† University of Western Australia, Australia.
‡ Cambridge University Engineering Department, Trumpington Street, Cambridge, UK.
§ Department of Civil and Environmental Engineering, University of Southampton, UK.

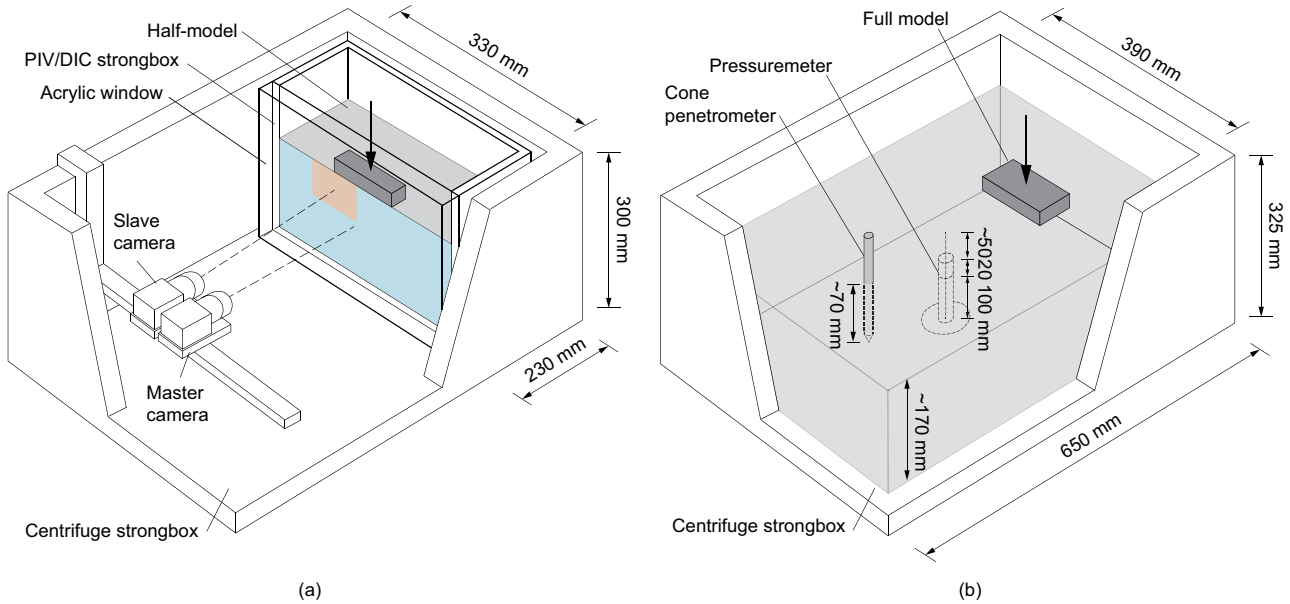

Fig. 1. Schematic diagram of centrifuge test set-up: (a) half-model test; (b) full-model test

Half-foundation-model test for PIV/DIC

The half-model rectangular foundation was fabricated with dimensions $L \times B$: 100×25 mm from anodised aluminium with coarse silica sand ($D_{50} = 0{\cdot}5$ mm) glued to the base to increase foundation roughness. This foundation was placed with the long side parallel to the transparent acrylic window of a $330 \times 230 \times 300$ mm PIV/DIC strongbox that fits within the standard centrifuge strongbox. The PIV/DIC strongbox has a transparent acrylic window on one face to expose a plane of the soil sample (see Fig. 1(a)). The thickness of the transparent window (50 mm) was sized following the recommendations in Haigh & Madabhushi (2014) that the deflected boundary should have minimal impact with respect to soil disturbance, especially for the in situ stress ratio condition. The acrylic window is rigidly connected against the two side walls and the base plate such that the maximum deflection of the window at the free top end can be calculated using elastic methods. This was calculated as less than 0·2 mm ($< 0{\cdot}001$ window height) for the current tests. Increasing the window stiffness also reduces photogrammetric distortion and improves the measurement precision of the PIV/DIC analysis, and allows half-foundation-model tests to be conducted at higher bearing pressures reliably. During the tests the foundation was loaded vertically at a constant vertical displacement rate of 0·01 mm/s until the column type load cell (De Catania *et al.*, 2010) reached its capacity of 8 kN.

An in-house developed synchronised multi-scale image capture system using two cameras was used to capture the deformation mechanisms in two series of images at 'macro' and 'micro' scales (Fig. 2). A central camera records the full field of view (FoV) of the PIV/DIC test capturing the 'macro' deformation mechanism and the boundaries of the model. An adjacent slave camera simultaneously records a smaller 'micro' FoV near the foundation, capturing deformations close to the foundation at higher definition. In brief, the hardware consists of: two 5-megapixel cameras (Allied Vision Technologies Prosilica GC2450); a pair of light-emitting diode (LED) panels (CCS Industries Ltd, model number LDL2-266X30SW-WD) to provide lighting; and in-house control units that supply power and commands to the lighting and cameras, respectively.

In-house software was developed to control the cameras, lighting and an image analysis module GeoPIV-RG (Stanier *et al.*, 2015) and incorporates a first-order subset shape function, bi-quintic b-spline image intensity interpolation and inverse compositional Gauss–Newton subset deformation parameters opimisation. See Teng *et al.* (2016) for more comprehensive details on the hardware and software for this multi-scale PIV/DIC system.

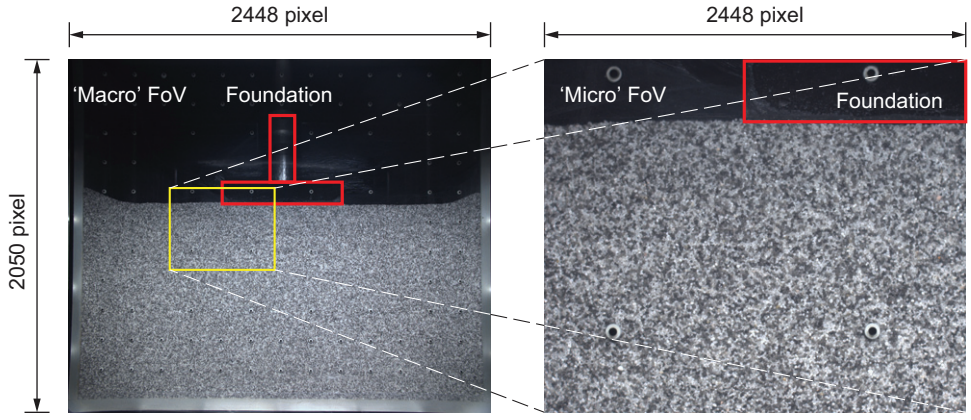

Fig. 2. 'Macro' FoV of master camera and 'micro' FoV of slave camera

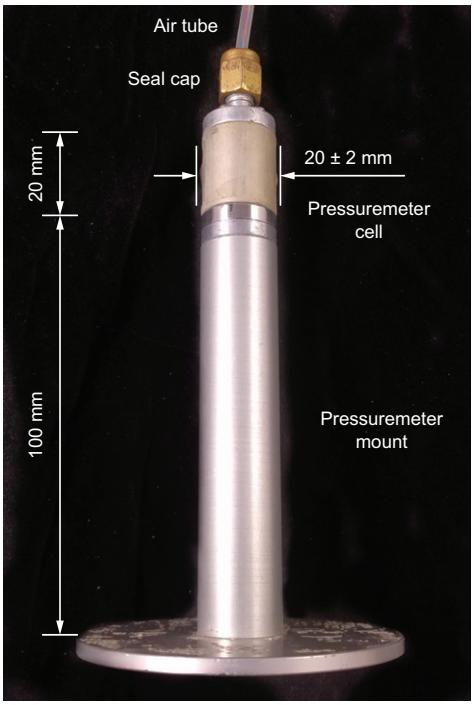

Fig. 3. Pre-buried pressuremeter on mount

Full-foundation-model test

The full-model rectangular foundation was fabricated with dimensions $L \times B$: 100 × 50 mm from anodised aluminium with silica sand glued at the base to increase foundation roughness – as for the half-model. The experiments were performed in a standard full-size strongbox ($L \times B \times D$: 650 × 390 × 325 mm) under the same conditions as the half-model tests, including rate of loading. Owing to the additional space available, it was possible to perform miniature cone penetrometer tests (CPTs) and pre-buried miniature pressuremeter tests (PMTs; see Fig. 3) to provide measurements of strength and stiffness for each of the samples (Stewart & Randolph, 1991; Johnston *et al.*, 2013; Teng, 2018). Placement of the instruments in the strongbox is indicated in Fig. 1(b).

A single foundation size of 50 mm × 100 mm model scale, 2·5 m × 5 m at prototype scale, was considered in this study since previous centrifuge testing has shown no significant scale effect for circular shallow foundations on carbonate sands considering foundation diameter varying from 1 m to 10 m at prototype scale (Finnie, 1993).

SAND SAMPLES

A commercially available coarse silica sand and two natural carbonate sands were tested. The coarse silica (CS) sand with relatively uniform particle size and shape was sourced from a commercial supplier (Sibelco Group, Australia). One of the carbonate sands was from an onshore location at Ledge Point (LP) in western Australia (Sharma & Ismail, 2006) and has a high calcium carbonate content of more than 90%. A second carbonate sand, recovered from the Goodwyn (GW) field located offshore north-western Australia (Sharma & Ismail, 2006), was considered as the third sand type for this study, as although it has a similar particle size distribution to the Ledge Point carbonate sand, it is more crushable, with the particles breaking between fingers.

Volumes of both the coarse silica sand and Ledge Point sand were dyed black and mixed with undyed sand in order to enhance the captured image contrast, such that the artificial seeding ratio (ASR) was approximately 0·5, following the recommendations in Stanier & White (2013). Trials of dying the Goodwyn sand to achieve optimal image contrast proved unsatisfactory, as dye was absorbed into intra-particle voids rather than coating the outer particle surfaces. The Goodwyn sand is very uniform in colour, which makes for suboptimal PIV/DIC analyses due to the low image contrast causing poor correlations. As an alternative to dyeing, the Goodwyn sand was mixed in a 50/50 ratio with the Ledge Point sand, which has a highly contrasting particle colour. This created a second carbonate sample that had high spatial contrast on the exposed plane of the model and so was well suited to PIV/DIC analysis.

All samples (whether in PIV/DIC or full-size strongboxes) were pluviated using a dry sand raining machine with the sand poured from a bar hopper with constant opening and fall height, as the hopper moved back and forth along the strongbox at a constant rate. The same fall height and lateral travel rate were used for all samples tested. Sample density was determined by measuring total weight and total volume, and relative density D_r was determined by maximum/minimum index density and sample density. The relative density D_r in the coarse silica sand was 84% (dense), and for the carbonate sands the relative density was 52% and 55% (medium-dense) for the LP and GW/LP sands, respectively. Sampling trials were carried out to investigate whether denser carbonate samples could be achieved with dry pluviation, but this was not possible. Additional vibratory compaction was also considered but ultimately dismissed on the grounds that it might cause particle breakage. Since all the samples were dense or medium-dense and the purpose of the programme of tests was to illustrate and explain different responses, the variation in relative density was not considered an issue and adoption of consistent fall height during pluviation became the preferred method of sample preparation. In essence this is modelling the impact of sedimentation of different sediments in the same environment.

The Goodwyn carbonate sand and Ledge Point carbonate sand in the GW/LP carbonate sample was well mixed, but slight stratification of the two sands was unavoidable due the different unit weight of the two constituent sands and the dry pluviation process.

The critical state angle of friction, ϕ'_{cr}, was determined by the Cornforth method (Cornforth, 1973), indicating similar values for all three sands, although slightly higher for the carbonate sands.

The particle size distributions of the three sand samples are shown in Fig. 4 and Table 1 presents values of key

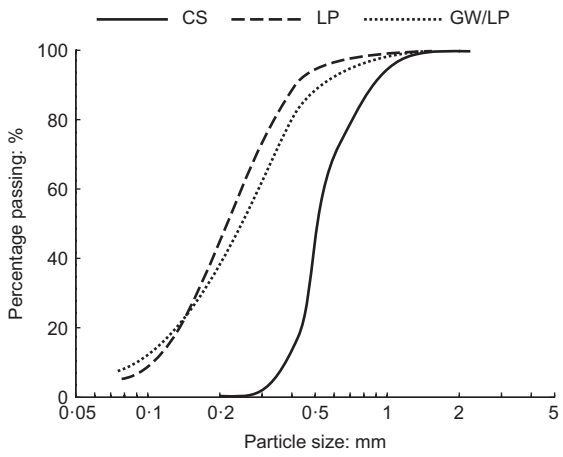

Fig. 4. Particle size distribution of sand samples: CS, coarse silica sand; LP, Ledge Point sand; and GW/LP, Goodwyn/Ledge Point sand

Table 1. Key geotechnical characteristics of the sands used in the centrifuge models

Sand	Sample density, ρ: kg/m^3	Specific gravity, G_s: –	Max. void ratio, e_{max}: –	Min. void ratio, e_{min}: –	Relative density, D_r: %	D_{50}: mm	Uniformity coefficient, C_u	Critical state angle of friction, ϕ'_{cr}: deg
Coarse silica sand (CS)	1760	2·65	0·69	0·47	84	0·51	1·38	33·0
Ledge Point carbonate sand (LP)	1400	2·76	1·17	0·80	52	0·21	2·67	35·0
Goodwyn/Ledge Point carbonate sand (GW/LP)	1330	2·74	1·28	0·88	55	0·24	3·11	35·5

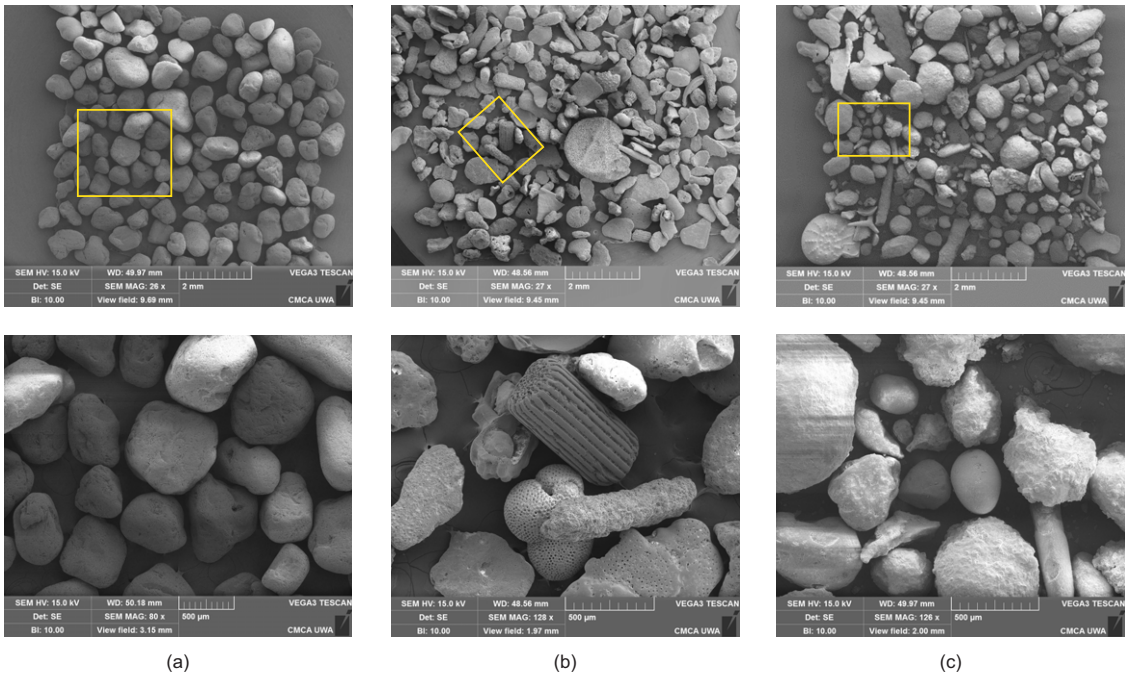

Fig. 5. Particle shape of samples under scanning electron microscope: (a) CS sand; (b) LP carbonate sand; and (c) GW/LP carbonate sand

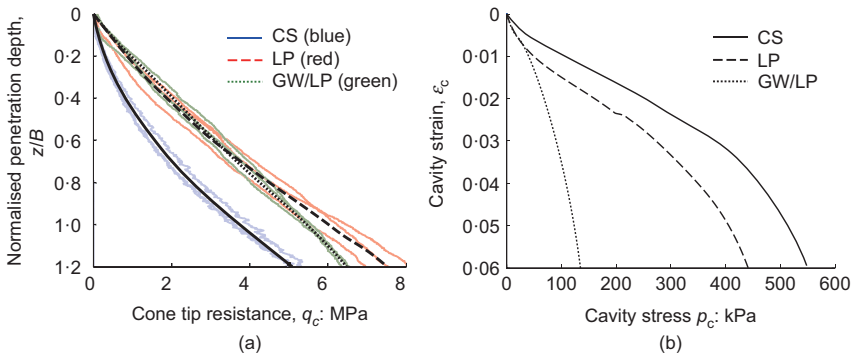

Fig. 6. (a) Cone penetration tests, three in each sand sample; (b) pressuremeter tests of the three sand samples. A full-colour version of this figure can be found on the ICE Virtual Library (www.icevirtuallibrary.com)

geotechnical characteristics for each of the samples. All samples are poorly graded ($C_u < 6$) with the median particle size D_{50} of CS, LP and the GW/LP sands being 0·51, 0·21 and 0·24 mm, respectively. Scanning electron microscopy (SEM) was used to observe the particle shape of the different samples (Fig. 5). The coarse silica sand particles are mostly rounded with a smooth surface. The LP carbonate sand and the GW/LP sand have a high portion of highly angular particles, and GW/LP sand also contains hollow and highly crushable particles.

MINIATURE CONE PENETROMETER AND PRESSUREMETER TEST DATA

Figure 6(a) presents the cone penetrometer resistance profile with normalised penetration depth by foundation width ($B = 50$ mm). Three CPTs have been conducted in each sand sample and all showed a consistent cone resistance profile. Fig. 6(b) presents the cavity stress–strain response from the pressuremeter tests, in which the pressuremeter cell was buried about 1B (50 mm) beneath the soil surface (Fig. 1(b)).

Distinct variations in trend can be observed with the coarse silica sand mobilising the lowest resistance in the

penetration test and the highest resistance in cavity expansion. Further, the magnitude of penetration resistance of the two carbonate samples are similar to each other, while the cavity expansion responses are quite different. Comparison of the trends observed in these characterisation tests are discussed further with respect to the observed foundation load–settlement response in the following section.

All the foundation tests and in situ tests in the centrifuge followed the requirements of the scaling laws and commonly accepted reference values for minimal scale effect as set out by Garnier *et al*. (2007).

SHALLOW FOUNDATION BEARING RESPONSE

Figure 7 presents a comparison of the load–displacement response from the half- and full-model tests in each sand, illustrating that the load-bearing responses from the two types of test are similar (to within 14% of each other) up to a normalised settlement (s/B) of 10%. This provides confidence that the mechanisms observed in the half-model PIV/DIC tests is a realistic representation of the mechanisms generated under the full-model tests, alleviating concerns of boundary impacts caused by friction between the foundation, soil and transparent acrylic window. The full-model and half-model foundation load–displacement response in the three sands are compared in Fig. 8.

The foundation bearing resistance is highest in the coarse silica sample and lowest in the mixed Goodwyn and Ledge Point sample. Foundation bearing capacity is taken at a normalised foundation displacement $s/B = 10\%$ (5 mm model scale, 0·25 m prototype scale) to enable comparison. The ultimate bearing resistance in CS sand is then 950 kPa, followed by LP carbonate sand at 800 kPa and GW/LP carbonate sand at 600 kPa. It is interesting to note that the foundation bearing response trends are contrary to the CPT resistance trend, which implied that the carbonate sands had higher strength, yet in these results the carbonate sands exhibit lower foundation bearing resistance than the silica sand. In contrast, the trend in bearing capacity mobilised in the foundation tests is the same as the trend in the resistance observed in the miniature pressuremeter tests (PMT). This implies that the deformation mechanism generated by the PMT is more akin to that generated beneath a shallow foundation under vertical loading on carbonate sand than that generated by cone penetration. A summary of these trends is presented in Table 2 and the observations are discussed further in the context of the observed deformation mechanisms within the soil mass in the following section.

SOIL DEFORMATION MECHANISMS

Displacement and strain fields observed on the exposed plane of the half-model tests in the 'macro' view, derived from the multi-scale synchronised PIV/DIC analysis, are plotted for each of the sand samples in Figs 9 and 10, respectively, at normalised foundation displacement (s/B) of 1%, 2·5%, 5% and 10%. Positive displacements indicate settlement, whereas negative displacements indicate heave.

Figure 9 indicates that the carbonate sands mobilise a mechanism that is quite different to the silica sand. Generally, for

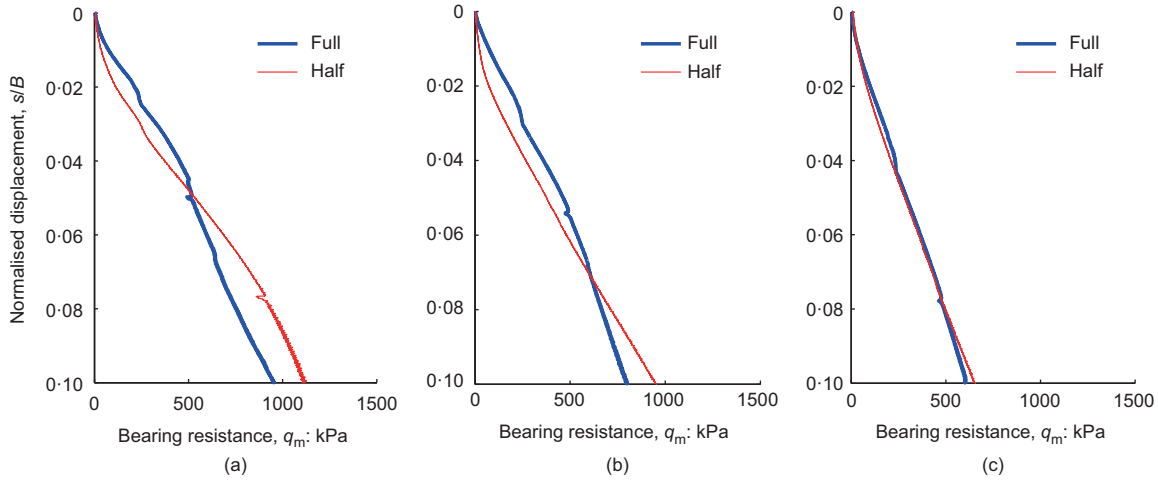

Fig. 7. Comparison of full and half foundation model load–displacement response: (a) CS sand; (b) LP sand; (c) GW/LP sand

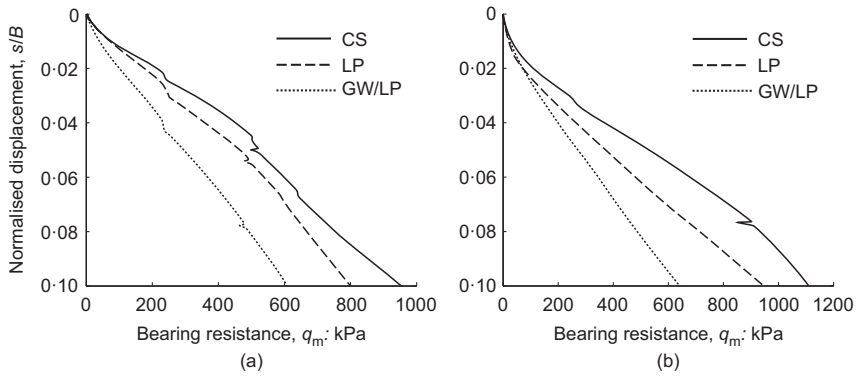

Fig. 8. Comparison of foundation model load–displacement response on different sands: (a) full-model tests and (b) half-model tests

Table 2. Comparison of trends in soil response in different tests

Test	Measure	Result (high to low)
Cone penetrometer test	Cone tip resistance, q_c, at given penetration depth	LP ≈ GW/LP > CS
Pressuremeter test	Cavity stress, p_c, at given cavity strain	CS > LP > GW/LP
Foundation test	Bearing resistance, q_m, at given displacement	CS > LP > GW/LP

all settlement increments, the silica sand mechanism is relatively shallow with significant lateral displacement of soil at the corner of the foundation and significant heave adjacent to it. In contrast, for the carbonate sands, the lateral displacements are smaller in magnitude, there is no heave adjacent to the foundation, and the mechanisms extend to a slightly greater depth into the soil mass. The GW/LP sand also generates a more vertically expanded mechanism, predominantly confined to the area beneath the foundation. Such contrasting mechanisms can be differentiated at the very beginning of the tests (Figs 9(a1), 9(b2) and 9(c1)) and the differences become more pronounced as the displacement increases.

Figure 10 presents the corresponding shear and volumetric strain fields at the same settlement increments shown for the displacement contours in Fig. 9, which allow further scrutiny of the soil deformation mechanisms. Initially, at 1% s/B, the mechanisms do not look overly dissimilar (c.f. Figs 10(a1)–10(b1)–10(c1)) and referring to Fig. 8, the difference in bearing capacity between the three sands is modest. As the settlements increase, from 1% to 10% s/B (c.f. Figs 10(a2)–10(b2)–10(c2), 10(a3)–10(b3)–10(c3), 10(a4)–10(b4)–10(c4)), the contrast between the mechanisms becomes more marked – mirrored in the observed foundation load–settlement responses (Fig. 8). The carbonate sands undergo significant volumetric compression immediately beneath the foundation, with the mechanisms also extending to greater depth. This volumetric compression is particularly evident for the GW/LP sand, which contained a large fraction of the highly crushable Goodwyn sand particles.

Based on the well-established descriptions of potential failure mechanisms for shallow foundations subjected to vertical loading (Vesic, 1974), the mechanism in the coarse silica sand is close to what is described as the 'general shear failure mode', while the 'punching shear failure mode' is closest to the mechanisms observed in the LP carbonate sand and GW/LP carbonate sand tests. The more readily crushable Goodwyn sand grains in the GW/LP soil amplified the difference in mechanisms by generating more volumetric compression beneath the foundation than in the LP soil, which leads to even smaller lateral components of displacement in the mechanism resulting in a 'punching shear failure'

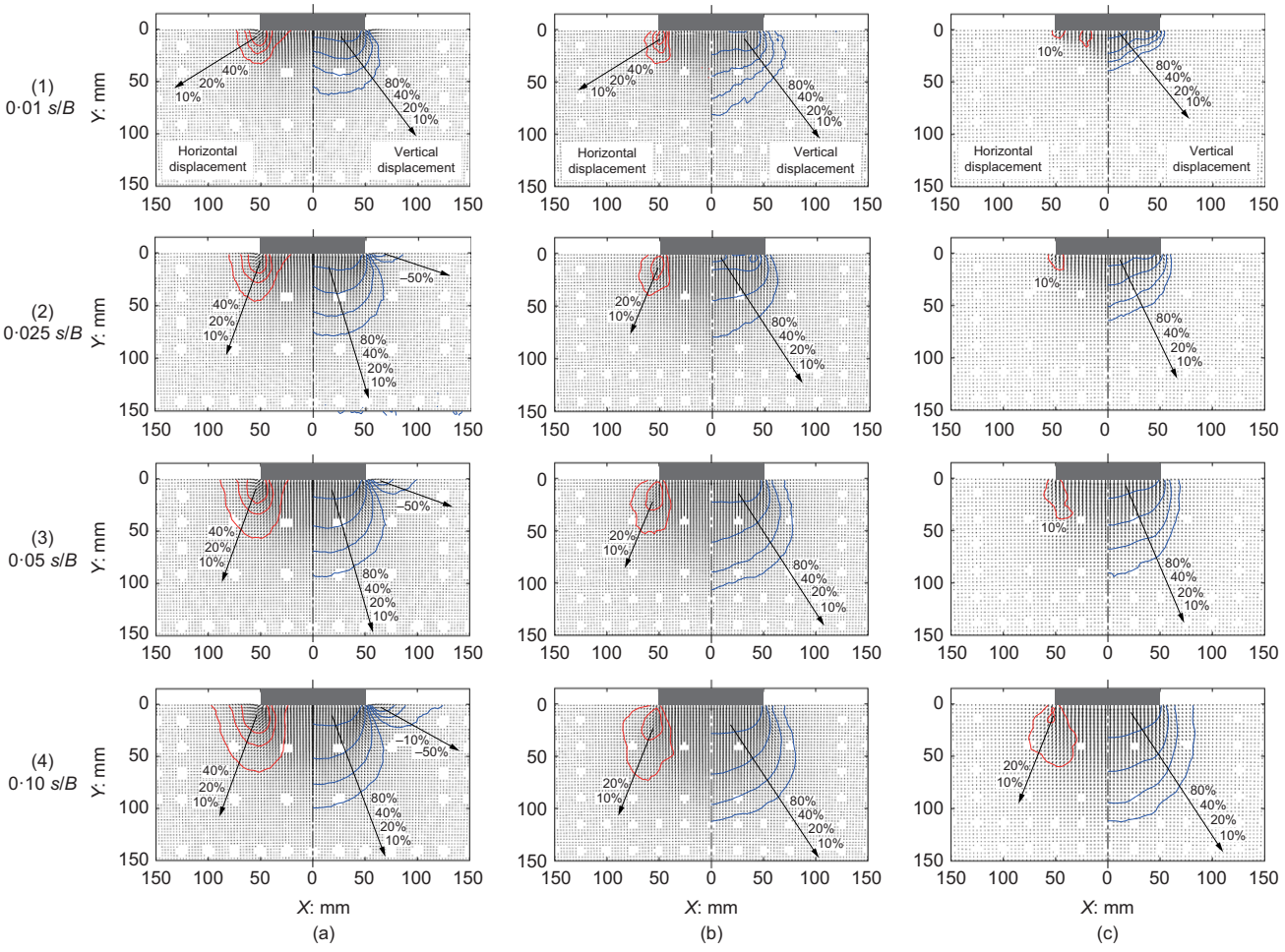

Fig. 9. Velocity vectors and normalised displacement contour fields at (1) 0·01 s/B, (2) 0·025 s/B, (3) 0·05 s/B and (4) 0·1 s/B: (a) CS sand; (b) LP sand; (c) GW/LP sand – Macro FoV

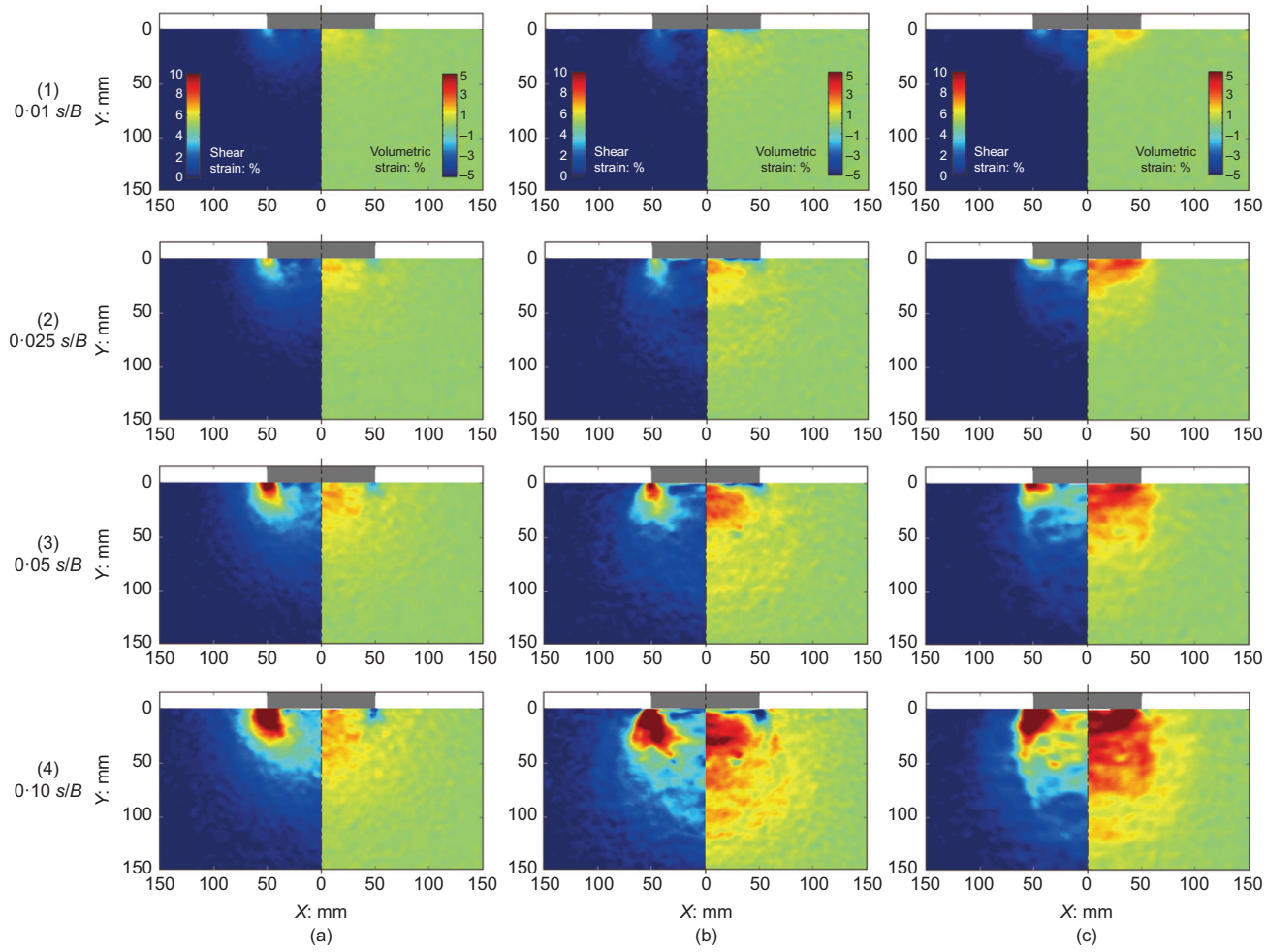

Fig. 10. Shear strain fields and volumetric strain fields at (1) 0·01 *s/B*, (2) 0·025 *s/B*, (3) 0·05 *s/B* and (4) 0·1 *s/B*: (a) CS sand; (b) LP sand; (c) GW/LP sand. A full-colour version of this figure can be found on the ICE Virtual Library (www.icevirtuallibrary.com)

mode. The particle crushing also led to a lower bearing capacity being generated in the GW/LP sand compared to the LP sand, even though both materials have very similar critical state friction angles.

The strain fields show that the coarse silica sand is the least compressible of the three sands tested, which is partially due to the higher relative density, but also to the absence of particle crushing occurring beneath the foundation. Fig. 11 shows the volumetric strain measurements at 10% *s/B* in all three sands, as measured by the 'micro' view camera. This camera captures a reduced FoV at ~20 times the resolution of the 'macro' view camera. The CS sand (see Fig. 11(a)) exhibits small pockets of volumetric compression and expansion that are masked in the lower resolution 'macro' view images. These pockets of volumetric strain are consistent with local changes in density that are generated as the sand is sheared from its initial (pluviated) void ratio, towards the critical state void ratio for the apparent stresses at that location in the mechanism. At the corners of the foundation, where the contact stresses will tend to be smallest, a modest amount of localised dilation is also evident.

In contrast, the LP sand (Fig. 11(b)) exhibits significant volumetric compression immediately beneath the foundation. This can potentially be attributed to: (*a*) rearrangement of particles into a denser packing structure; and (*b*) crushing of hollow particles. The LP sand does not exhibit a significant tendency to crush under the magnitude of stresses applied to the shallow foundation in the model tests, hence most of the volumetric strains are thought to be caused by particle rearrangement, which is encouraged by the proliferation of flat particles in the soil particle assembly (see Fig. 5(b)).

The GW/LP mix has a higher tendency for particle crushing to occur due to the highly crushable nature of the Goodwyn sand particles. The slight sample stratification – as mentioned earlier – highlights the impact of the presence of the highly crushable Goodwyn sand particles in the soil particle assembly: Fig. 11(c) shows that the layers predominantly composed of Goodwyn sand generate more volumetric compression than the layers predominantly comprising Ledge Point sand particles.

For both of the carbonate sands (Figs 11(b) and 11(c)), a large volume of soil experiences dilation at the corner of the foundation. This is consistent with lower stresses being generated in the soil in these zones, which is caused by the reduced confinement which results from the mechanism not extending laterally outwards from the corner of the foundation. In other words, for the carbonate sands, it is easier for the foundation to mobilise the soil beneath rather than adjacent to the foundation.

The PIV/DIC analyses illustrate that there are different deformation mechanisms occurring in each of the different sand samples. The strain field measurements indicate that the behaviour of each of the sands is quite different, with silica sands undergoing modest volumetric changes due to localised particle rearrangement and the carbonate sands undergoing more significant volumetric compression due to particle rearrangement (LP) and particle crushing (GW/LP).

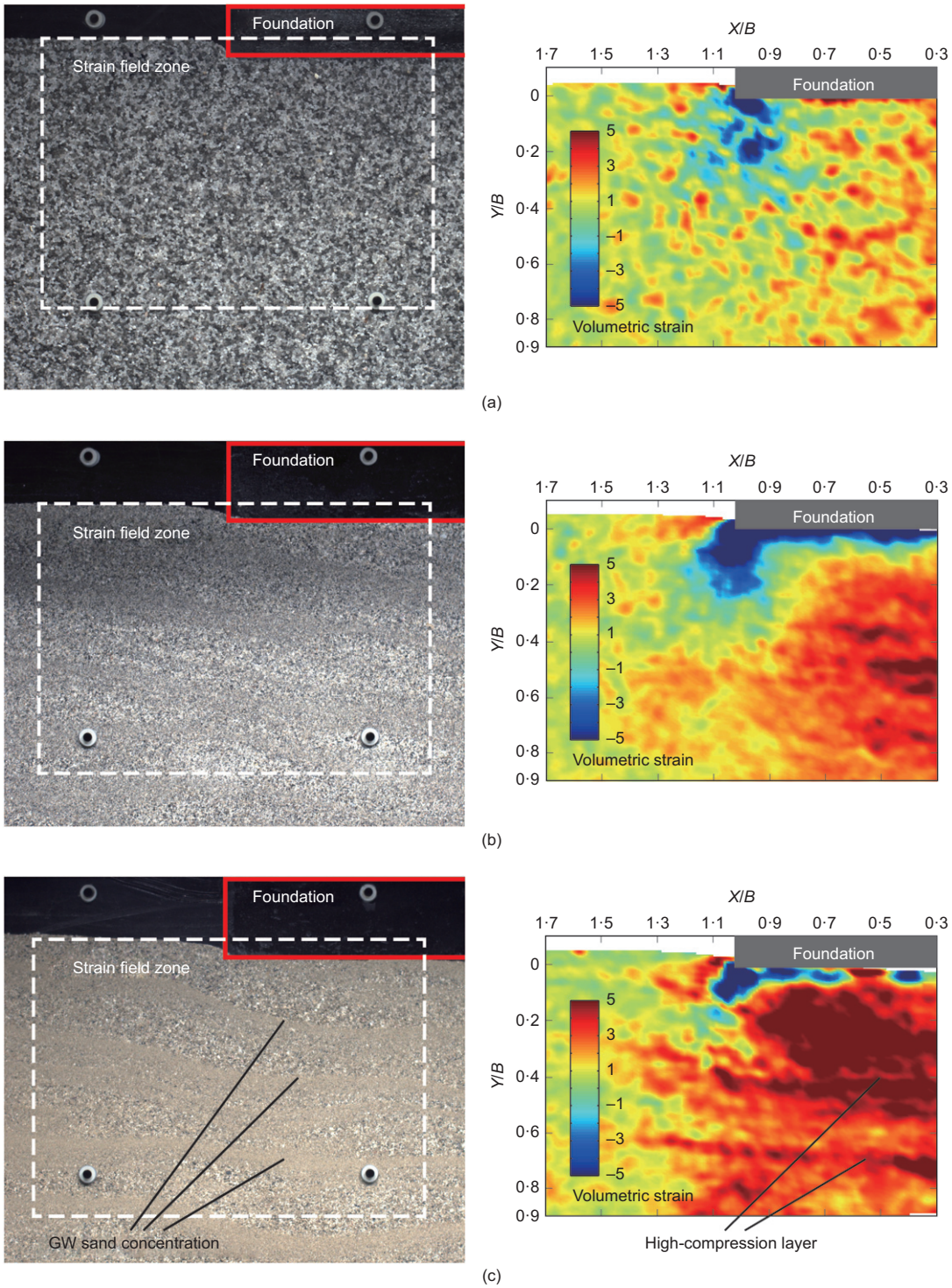

Fig. 11. Volumetric strain field measurement at 10% *s*/*B* using 'micro view' image: (a) CS sand; (b) LP carbonate sand; and (c) GW/LP carbonate sand. A full-colour version of this figure can be found on the ICE Virtual Library (www.icevirtuallibrary.com)

This is evidence that sands do not behave as a perfect continuum, hence particle shape effects and interparticle behaviour should be considered, especially at regions near geo-structures, where these effects will be magnified.

POTENTIAL PARTICLE SHAPE EFFECT

Particle shape is a key factor in understanding particle and interparticle behaviour and is explored here to explain the differences observed in the different sands tested in this study.

Two measures of particle characteristic, namely, sphericity (S) and roundness (R), are used to describe the shape or geometric form of particles (Krumbein & Sloss, 1963). Sphericity S describes the ratio of the largest inscribed sphere to the smallest circumscribed sphere of a particle and is a scalar reflection of the similarity between the particle's length, height and width. Roundness R is a measurement of particle boundary features using the maximum projected area of a particle, expressed as the ratio of the average radius of the corners and the edges to the radius of the maximum inscribed circle of the projected area of the particle from a given viewpoint.

A reference for visual estimation of sphericity and roundness is given in Fig. 12 (after Krumbein & Sloss, 1963).

The SEM images of the three sand samples (Fig. 5) provide appropriate detail for estimations of S and R, which are summarised in Table 3. Since sphericity and roundness can have a wide measurement range in carbonate sands, the current authors' estimated values are averaged values for ~100 particles in the SEM images for each of the sand samples.

Sphericity and roundness are very high in CS sand, but much lower in LP carbonate sand and GW/LP carbonate sand. Low roundness can result in high values of maximum and minimum void ratios (Youd, 1973), supported by a particle shape database summarised by Cho *et al.* (2006) and shown in Table 4. The present study's measurements of maximum and minimum void ratio, presented in Table 1, follow this trend and the observed compressibility of the sands as measured in the volumetric strain fields in Figs 10 and 11 clearly increases with reducing roundness and sphericity. In contrast, the critical friction angle ϕ_{cr} does not have very strong correlation with either sphericity or roundness, or – at least in this investigation – with the bearing capacity of the sand.

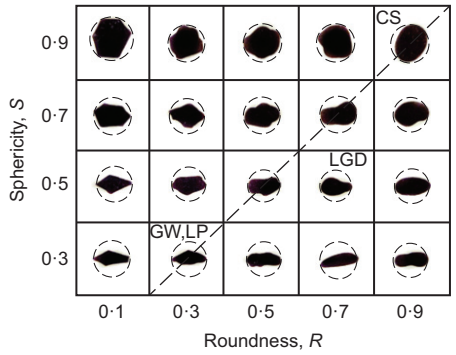

Fig. 12. Visual reference for estimation of sphericity and roundness

The distribution of lateral and vertical components in displacement fields that govern the type of bearing capacity mechanism formed can also potentially be attributed to particle shape effects. Since the foundation load was vertical in these tests, any lateral displacement in the soil mass must arise from foundation load being transferred laterally through the interparticle contacts. The magnitude of the lateral component of displacement in the deformation mechanism also increases with increasing sphericity and roundness. The pluviation sampling process of sand, which is similar to a natural deposition process, is likely to result in particles being mainly oriented horizontally, especially for medium dense to dense samples as tested in this investigation. Fig. 13 illustrates the probable load transfer directions between idealised assemblages of horizontally oriented particles with different roundness R (and technically, as a result, sphericity S), showing that a higher proportion of load is transferred horizontally when the particles are more rounded. For the carbonate sand, the highly angular particle shape resulted in low sphericity and roundness, causing the load to be predominantly transferred vertically. Owing to

Table 3. Particle shape parameters and soil behaviour comparisons

Sand	Sphericity, S	Roundness, R	Compressibility	Crushability	Ratio of lateral component in total displacement
Coarse silica sand (CS)	~0·9 (high)	~0·9 (high)	Lowest	Low	Highest
Legendre sand, Teng *et al.* (2017)	~0·5 (med.)	~0·7 (med.)	Low	Low	Medium
Ledge Point sand (LP)	~0·3 (low)	~0·3 (low)	High	Low	Low
Goodwyn/Ledge Point sand (GW/LP)	~0·3 (low)	~0·3 (low)	Highest	High	Lowest

Table 4. Database of soil properties of sand samples (after Cho *et al.*, 2006)

Sand sample	Sphericity, S	Roundness, R	e_{max}	e_{min}	Critical friction angle, ϕ_{cr}: deg
Glass beads	1·00	1·00	0·72	0·54	21
Coarse silica*	0·90	0·90	0·85	0·51	33
Ottawa #20/30	0·90	0·90	0·72	0·50	27
ASTM graded	0·90	0·80	0·82	0·50	30
ASTM 20/30	0·90	0·80	0·69	—	32
Michigan Dune	0·87	0·77	0·80	0·56	29
Nevada	0·85	0·60	0·85	0·57	31
Ponte Vedra	0·85	0·30	1·07	—	39
Jekyll Island	0·85	0·30	1·04	—	40
Ottawa #20/70	0·81	0·76	0·78	0·47	28
Ticino	0·80	0·40	0·99	0·57	37
Ottawa #60/80	0·78	0·65	0·85	0·55	30
Margaret River	0·70	0·70	0·87	—	33
Ottawa F110	0·70	0·70	0·85	0·54	31
Daytona Beach	0·70	0·62	1·00	0·64	32
Sandboil	0·70	0·55	0·79	0·51	33
Ottawa #45	0·68	0·45	1·10	0·75	33
Syncrude Tailings	0·62	0·47	1·14	0·59	31
Ottawa #90	0·60	0·40	1·10	0·73	32
Blasting	0·55	0·30	1·03	0·70	34
Legendre†	0·50	0·70	0·84	0·51	36·5
Fraser River	0·50	0·25	1·13	0·78	35
Ledge point*	0·30	0·30	1·17	0·8	35
Goodwyn/Ledge Point*	0·30	0·30	1·28	0·88	35·5
Granite powder	0·24	0·40	1·30	0·48	34

*Present study.
†Teng *et al.* (2017).

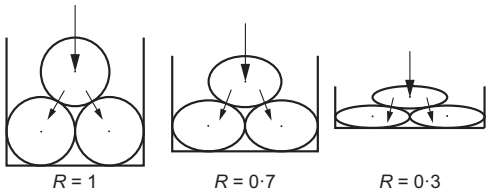

Fig. 13. Schematic representation of load transfer between idealised particles with different roundness

the higher initial void ratio and reduced lateral load transfer, the LP and GW/LP carbonate sands would be predicted to be more likely to generate a punching shear failure mechanism under vertical foundation load, as was observed. The more rounded coarse silica sand likely experiences increased lateral load transfer, leading to soil heave adjacent to the foundation (see Fig. 9(a)). The findings presented in this paper also agree well with the effect of particle shape observed by Rothenburg & Bathurst (1992), who studied the impact of eccentricity of elliptical particles on granular assemblage behaviour. They found that the eccentricity had a significant impact on the deformation characteristics, in particular the tendency for dilation. The cause of sample strength change was correlated with the number of interparticle contacts and directions, which were also related to the eccentricity. However, void ratio did not show a clear correlation with sample strength.

Another carbonate sand with predominantly plate-shaped particles at medium sphericity (0·5) and roundness (0·7), Legendre sand, has been tested and compared with CS sand and Ledge Point sand in a strip foundation testing campaign (Teng *et al.*, 2017). Those tests showed that the more spherical and rounded Legendre sand (compared to the other carbonate sands) generated more significant lateral components of displacement than the other carbonate sands, but still not as much as the silica sand, which has the most spherical and rounded particles of the sediments tested. This also supports the observations regarding the influence of particle shape in this paper. A comparison of particle shape characteristics and component of lateral load transfer observed in the bearing capacity mechanism is presented in Table 3.

CONCLUSIONS

Shallow foundation response under vertical loading in three different sands, one silica and two carbonate sands, has been investigated through a programme of centrifuge model tests. The sand samples were prepared using a consistent procedure, which resulted in samples of differing relative density for each of the sands; very dense for the silica sand and medium dense for the carbonate sands. This was not seen to be problematic when comparing the behaviours observed in the different tests as – in essence – this is modelling the impact of sedimentation of different sediments in the same environment. Full-model and half-model tests provided data on foundation load–settlement response and soil deformation mechanisms in micro and macro fields of view that enabled scrutiny of the vertical and horizontal components and shear and volumetric components of the failure mechanisms. Miniature CPTs and pressuremeter tests enabled assessment of the applicability of cone resistance and pressuremeter cavity expansion to capture the governing soil response under the foundation.

The SEM images enabled the influence of particle shape on the observed soil response to be considered.

The programme of work showed the following.

(*a*) The trend in the magnitude of the net CPT resistance was different to that of the foundation resistance for the silica and carbonate sands. The carbonate sands, which have a slightly higher friction angle than the silica sand, generated the highest net CPT resistance, while in contrast, mobilised the lowest foundation bearing resistance.

(*b*) The trend in the magnitude of the PMT stress–strain response agreed more closely with the trend of the bearing response in the foundation tests, with the silica sand mobilising the highest resistance, followed closely by the LP carbonate sand, with the GW/LP carbonate sand mixture mobilising the lowest resistance. The carbonate sands generated the lowest cavity stress and bearing capacity in spite of having a slightly higher critical state friction angle than the silica sand.

(*c*) The propensity for carbonate particles to crush under load can have a significant effect on the bearing resistance mobilised by a shallow foundation. Adding highly crushable Goodwyn carbonate sand to the LP carbonate sand resulted in a significant reduction in bearing resistance, in spite of the friction angle and relative density being approximately the same in the two sands.

(*d*) Particle shape effects have been proposed to contribute to the different deformation mechanisms observed beneath the shallow foundations. Particle shape parameters, sphericity and roundness, are determined from SEM images and fit well with the existing database linking the magnitudes of the maximum and minimum void ratios of a particle assembly, and potentially the load transfer directions between particles. Low sphericity and particle roundness appear to promote punching shear failure modes over general shear failure modes that involve more significant lateral mobilisation of soil at failure.

The findings of this study provide insights into shallow foundation response in different sands through synthesis of results from centrifuge model testing, synchronised multi-scale PIV/DIC analysis and SEM. The results highlight the significance of particle shape on the load transfer mechanism and subsequent global failure mechanism and show that pressuremeter tests, as opposed to more conventional cone penetrometer tests, may provide a more representative load path for determining an appropriate input parameter for a predictive model for bearing response. The results provide insights and cautions to inform the geotechnical design of shallow foundations on carbonate sands and provide a valuable high-quality data set to contribute to the development of a theoretical or constitutive model to better represent the geotechnical response of carbonate soils.

ACKNOWLEDGEMENTS

This work forms part of the activities of the Centre for Offshore Foundation Systems (COFS) – established in 1997 under the Australian Research Council's Special Research Centres Program; supported as a node of the Australian Research Council's Centre of Excellence for Geotechnical Science and Engineering, and through the Fugro Chair in Geotechnics, the Lloyd's Register Foundation Chair and Centre of Excellence in Offshore Foundations and the Shell EMI Chair in Offshore Engineering. The work presented in this paper was supported through ARC grant CE110001009. This support is gratefully acknowledged. The authors thank Dr James Doherty for his loan of the miniature pressuremeter for the centrifuge tests; Mr John Breen and Miss Khin Thida Seint for developing and maintaining hardware and software for centrifuge testing; Mr Manuel Palacios for his assistance during the centrifuge experiments. The

authors also acknowledge the facilities and assistance of the Australian Microscopy & Microanalysis Research Facility at the Centre for Microscopy at UWA.

NOTATION

B	width of the model foundation or strongbox
D	depth of the strongbox
$D50$	sieve size at which 50% weight of sample pass through
D_r	relative density of soil sample
e_{max}	maximum void ratio of soil sample
e_{min}	minimum void ratio of soil sample
G_s	specific gravity of soil sample
$\boldsymbol{g}$	acceleration due to gravity
L	length of the model foundation or strongbox
p_c	cavity stress of pressuremeter
q_c	cone tip resistance of cone penetrometer
R	average roundness of soil sample
S	average sphericity of soil sample
z	cone penetration depth
ε_c	cavity strain of pressuremeter
ρ	density of soil sample
ϕ_{cr}	critical state friction angle (or friction angle for constant volume shearing)

REFERENCES

Bolton, M. D., Gui, M. W., Garnier, J., Corte, J. F., Bagge, G., Laue, J. & Renzi, R. (1999). Centrifuge cone penetration tests in sand. *Géotechnique* **49**, No. 4, 543–552, https://doi.org/10.1680/geot.1999.49.4.543.

Cho, G. C., Dodds, J. & Santamarina, J. C. (2006). Particle shape effects on packing density, stiffness, and strength: natural and crushed sands. *Journal of Geotechnical and Geoenvironmental Engineering* **132**, No. 5, 591–602.

Cocjin, M. & Kusakabe, O. (2013). Centrifuge observations on combined loading of a strip footing on dense sand. *Géotechnique* **63**, No. 5, 427–433, https://doi.org/10.1680/geot.11.P.075.

Coop, M., Sorensen, K., Bodas Freitas, T. & Georgoutsos, G. (2004). Particle breakage during shearing of a carbonate sand. *Géotechnique* **54**, No. 3, 157–163, https://doi.org/10.1680/geot.2004.54.3.157.

Cornforth, D. H. (1973). Prediction of drained strength of sands from relative density measurements. In *Evaluation of relative density and its role in geotechnical projects involving cohesionless soils* (eds E. T. Selig and R. S. Ladd), STP 523, pp. 281–303. West Conshohocken, PA, USA: ASTM International.

De Catania, S., Breen, J., Gaudin, C. & White, D. J. (2010). Development of a multiple axis actuator control system. In *Physical modelling in geotechnics (ICPMG 2010)* (eds S. Springman, J. Laue and L. Seward), vol. 1, pp. 325–330. Leiden, the Netherlands: CRC Press/Balkema.

Dijkstra, J., Gaudin, C. & White, D. J. (2013). Comparison of failure modes below footings on carbonate and silica sands. *Int. J. Phys. Modelling Geotech.* **13**, No. 1, 1–12, https://doi.org/10.1680/ijpmg.12.00004

Finnie, I. M. S. (1993). *Performance of shallow foundations in calcareous soil*. PhD thesis, Department of Civil Engineering, the University of Western Australia, Perth, WA, Australia.

Frossard, E. (1979). Effect of sand grain shape on interparticle friction; indirect measurements by Rowe's stress dilatancy theory. *Géotechnique* **29**, No. 3, 341–350, https://doi.org/10.1680/geot.1982.32.2.161.

Garnier, J., Gaudin, C., Springman, S. M., Culligan, P. J., Goodings, D., Konig, D., Kutter, B., Phillips, R., Randolph, M. F. & Thorel, L. (2007). Catalogue of scaling laws and similitude questions in geotechnical centrifuge modelling. *Int. J. Phys. Modelling Geotech.* **7**, No. 3, 1–23, https://doi.org/10.1680/ijpmg.2007.070301.

Gaudin, C., White, D. J., Boylan, N., Breen, J., Brown, T., De Catania, S. & Hortin, P. (2009). A wireless high-speed data acquisition system for geotechnical centrifuge model testing. *Measmt Sci. Technol.* **20**, No. 9, 095709.

Govoni, L., Gourvenec, S. & Gottardi, G. (2011). A centrifuge study on the effect of embedment on the drained response of shallow foundations under combined loading. *Géotechnique* **61**, No. 12, 1055–1068, https://doi.org/10.1680/geot.7.00109.

Haigh, S. & Madabhushi, G. (2014). Discussion of 'Performance of a transparent flexible shear beam container for geotechnical centrifuge modelling of dynamic problems by Ghayoomi, Dashti and McCartney'. *Soil Dynamics Earthquake Engng* **67**, 359–362.

Hansen, J. B. (1970). A revised and extended formula for bearing capacity. *Danish Geotech. Inst. Bull.* **28**, 5–11.

Islam, M. K. (1999). *Constitutive models for carbonate sand and their application to footing problems*. PhD thesis, University of Sydney, Sydney, Australia.

Johnston, G., Doherty, J. & Lehane, B. (2013). Development of a laboratory-scale pressuremeter. *Int. J. Phys. Modelling Geotech.* **13**, No. 1, 31–37, https://doi.org/10.1680/ijpmg.12.00011.

Krumbein, W. C. & Sloss, L. L. (1963). *Stratigraphy and sedimentation*, No. QE571K7. San Francisco, CA, USA: Freeman.

Meyerhof, G. G. (1951). The ultimate bearing capacity of foudations. *Géotechnique* **2**, No. 4, 301–332, https://doi.org/10.1680/geot.1951.2.4.301.

Pestana, J. M. (1994). *A unified constitutive model for clays and sands*. ScD thesis, Massachusetts Institute of Technology, Cambridge, MA, USA.

Randolph, M. F., Jewell, R. J., Stone, K. J. L. & Brown, T. A. (1991). Establishing a new centrifuge facility. In *Centrifuge '91: proceedings of the international conference* (eds H.-Y. Ko and F. G. McLean), pp. 3–9. Rotterdam, the Netherlands: Balkema.

Rothenburg, L. & Bathurst, R. J. (1992). Micromechanical features of granular assemblies with planar elliptical particles. *Géotechnique* **42**, No. 1, 79–95, https://doi.org/10.1680/geot.1992.42.1.79.

Sharma, S. S. & Ismail, M. A. (2006). Monotonic and cyclic behavior of two calcareous soils of different origins. *J. Geotech. Geoenviron. Engng* **132**, No. 12, 1581–1591.

Stanier, S. A. & White, D. J. (2013). Improved image-based deformation measurement in the centrifuge environment. *Geotech. Testing J.* **36**, No. 6, 1–14.

Stanier, S. A., Blaber, J., Take, W. A. & White, D. J. (2015). Improved image-based deformation measurement for geotechnical applications. *Can. Geotech. J.* **53**, No. 5, 727–739.

Stewart, D. P. & Randolph, M. F. (1991). A new site investigation tool for the centrifuge. In *Centrifuge '91: proceedings of the international conference* (eds H.-Y. Ko and F. G. McLean), pp. 531–538. Rotterdam, the Netherlands: Balkema.

Teng, Y. (2018). *Multiscale investigation of silica and carbonate sands under monotonic and cyclic loading*. PhD thesis, University of Western Australia, Perth, WA, Australia.

Teng, Y., Stanier, S. A. & Gourvenec, S. M. (2016). Synchronised multi-scale image analysis of soil deformations. *Int. J. Phys. Modelling Geotech.* **17**, No. 1, 53–71, https://doi.org/10.1680/jphmg.15.00058.

Teng, Y., Stanier, S. & Gourvenec, S. (2017). Analysis of failure mechanisms in silica and carbonate sands beneath a strip foundation under vertical loading. In *ASME 2017 36th international conference on ocean, offshore and arctic engineering – volume 9: offshore geotechnics*, paper OMAE2017-61130. New York, NY, USA: American Society of Mechanical Engineers.

Terzaghi, K. (1943). *Theoretical soil mechanics*. New York, NY, USA: Chapman and Hall Limited, John Wiley and Sons, Inc.

Vesic, A. S. (1974). Analysis of ultimate loads of shallow foundations: closure of discussion of original paper J. Soil Mech. Found. Div. Jan. 1973. 1F, 6R. J. GEOTECH. ENGNG. DIV. V100, N. GT8, 1974, P949–951. *Int. J. Rock Mech. Min. Sci. & Geomech. Abstr.* **11**, No. 11, A230.

Youd, T. L. (1973). Factors controlling maximum and minimum densities of sands. In *Evaluation of relative density and its role in geotechnical projects involving cohesionless soils* (eds E. T. Selig and R. S. Ladd), STP 523, pp. 98–112. West Conshohocken, PA, USA: ASTM International.

Zhu, F., Clark, J. I. & Phillips, R. (2001). Scale effect of strip and circular footings resting on dense sand. *J. Geotech. Geoenviron. Engng* **127**, No. 7, 613–621.